# Analysis on the Performance Improvement of Reciprocating Pump with Variable Stiffness Valve using CFD

G. Zhu and S. M. Dong†

*School of Mechanical Engineering, Yanshan University, Qin Huangdao, Hebei province, 066004, China*

†*Corresponding Author Email: ysudshm@163.com*

## ABSTRACT

As a key component of reciprocating pump, the valve has a significant influence on its performance. However, it is difficult for the existing valve to simultaneously solve the problems such as fatigue, erosion and cavitation in engineering application. In this paper, a solution to these problems of using variable stiffness spring is proposed. And three new structures of the valve are designed. Furthermore, based on Computational Fluid Dynamics (CFD) method, a three-dimensional dynamic simulation model considering fluid-structure interaction in the suction stroke of reciprocating pump is established by using dynamic grid technique and User-Defined Functions (UDF). The performance of these new valves are compared with that of conventional valve respectively. The result shows that the new valves have significant influence on the motion characteristics of the valve disc, flow field distribution and cavitation. Besides, the simulation and experimental results of the maximum lift are compared, and it is found that they are basically in agreement. The new structures provide a new research direction for improving the performance of reciprocating pump. Simultaneously, the above simulation method can also provide guidance for valve design, structural optimization and service life improvement.

## NOMENCLATURE

| | | | |
|---|---|---|---|
| $a_t$ | acceleration of the valve disc | | collapse of vapor bubbles |
| $F_p$ | fluid force produced by the pressure difference | $t$ | time |
| | | $v_p$ | motion velocity of plunger |
| $F_s$ | spring force | $x_p$ | plunger displacement |
| $F_0$ | preload of spring | $u_i,u_j,u_k$ | velocity of fluid in the $x_i$, $x_j$, $x_k$ direction |
| $g$ | gravity acceleration | $V_v$ | velocity of the gaseous phase |
| $h$ | lift of the valve disc | | |
| $h_0$ | initial deformation of spring | $\alpha_v$ | volume fraction of the gaseous term |
| $l$ | length of the connecting rod | $\rho_v$ | density of the gaseous phase |
| $k$ | spring stiffness | $\rho_l$ | density of the liquid |
| $m_s$ | mass of the valve disc | $\rho$ | mixed phase density |
| $n_b$ | number of bubble per unit fluid volume | $\lambda$ | link ratio |
| $p$ | liquid confining pressure | $\theta$ | crank angle |
| $p_v$ | internal pressure of the cavity | $\delta_{ij}$ | kronecker symbol $\delta_{ij}$= 1 for i = j |
| $R$ | crank radius | $\mu$ | dynamic viscous coefficient |
| $R_B$ | radius of the bubble | $\mu_t$ | turbulent viscosity |
| $S_e$ | mass transfer source terms connected to the growth of vapor bubbles | $\sigma$ | surface tension coefficient of the liquid |
| | | $\omega$ | crank angular velocity |
| $S_c$ | mass transfer source terms connected to the | | |

## 1. INTRODUCTION

Reciprocating pump, as a general hydraulic machinery, has been widely used in fertilizer, food, light industry, petrochemical and other industries. Because of its outstanding characteristics of high discharge pressure and work efficiency, it plays an irreplaceable role in some fields, such as application of drilling and fracturing in oilfield (Aleksandar *et al.,* 2016). However, large flow rate, high discharge pressure and complexity of working medium put forward higher requirements for the service life and stability of its structural components. The fatigue and erosion failure of the valve is particularly remarkable. Most obviously, the service life of it is almost the shortest among all wearing parts of a drilling reciprocating pump (Yang *et al.,* 2010). Simultaneously, the motion characteristics of the valve disc have a significant influence on the performance of the reciprocating pump. It has been proved that poor valve movement is the main cause of the valve failure and efficiency reduction (Ma *et al.,* 2018). In addition, cavitation during the suction stroke will deteriorate suction performance and reduce efficiency. Furthermore, local high pressure may occur when bubbles rupture near the wall, which may cause noise, vibration and erosion, seriously reduce service life of the valve (Luo *et al.,* 2016).

At present, reciprocating pump mainly adopts self-acting conical valve. Many experts and scholars have done a lot of research on it. Singh *et al.* (1987) bulit a system model for the analysis and simulation of a complete reciprocating pump installation, which took into account valve dynamics, cylinder thermodynamics, and acoustic pulsations in the suction and discharge piping. Lee *et al.* (2015) presented a new mathematical model for analysis and diagnosis of high-pressure reciprocating pump, which considered the flow interaction among the different cylinders. Pei *et al.* (2016) established an experimental system to directly acquire the motion parameters of valve disc, compared them with simulation result, and drew a conclusion that these simulation models have some limitations. However, most of the above models are based on certain assumptions, ignoring the process of fluid-structure interaction. And it is difficult for them to obtain the distribution characteristics of flow field. With the rapid development of CFD technique, many scholars have studied the dynamic opening process of the valve by internal visual simulation. Such as, Song *et al.* (2010) established a three-dimensional CFD model to study the fluid characteristics and dynamic behavior of a spring-loaded pressure safety valve. Moreover, Beune *et al.* (2012) developed a multi-mesh numerical valve model to analyze the opening characteristic of high pressure safety. Saha *et al.* (2014) investigated dynamic modeling of flow process inside a pressure regulating and shut-off valve using computational fluid dynamic approach. Qian *et al.* (2014) utilized CFD method combining dynamic grid technique to analyse internal flow field distribution and working principle of pilot-control globle valve. Ma *et al.* (2018) studied the whole working cycle of reciprocating multiphase pump by using CFD method. The lag characteristics of suction and discharge valves under different working conditions were analyzed in it. In addition, data-driven and hybrid modeling methods (Deng *et al.,* 2018a, b, c; 2019) also show obvious advantages for accurate description of the quick and nonlinear change of state parameters during reciprocating pump operation. However, they require sufficient and reliable data obtained by experiment or simulation. Although CFD method may need more computation time and reasonable model selection for complex problems, its calculation results contain more process and state information. It can not only obtain the motion characteristics of the valve disc, but also obtain the distribution of internal flow field, which has a good guiding significance for design and optimization of the valve in reciprocating pump.

Cavitation in pumps has been concerned near one century (Luo *et al.,* 2016). It will cause noise, vibration, erosion and malfunction in serious situation. With the help of high-speed camera measurements, Opitz *et al.* (2010) studied effects of cavitation in reciprocating pump. Lannetti *et al.* (2016) investigated, by means of CFD simulation method and experimental comparison, benefits and drawbacks of the 'full' cavitation model. Furthermore, Liang *et al.* (2016) analyzed the relationship between inlet pressure fluctuations and unsteady cavitation process condition inside a water hydraulic poppet valve using a two-phase mixture model. Kaya *et al.* (2017), considering cavitation is a major problem in pump design and operation, developed a systematic methodology to calculate the cavitation performance of radial flow pumps.

As an important part of self-acting conical valve, spring has obvious influence on the dynamic characteristics of the valve disc, suction performance and internal flow field distribution. Up to date, common cylindrical helical spring has been widely used in reciprocating pump. Its stiffness is approximately constant during the working process. Research has shown that increasing spring stiffness or preload is beneficial to reduce impact velocity and closing lag angle, but also reduces lift, increases resistance loss at the same time (Wang *et al.,* 2015), and will cause cavitation in severe situation, which deteriorates the suction performance. Therefore, it is difficult to balance the above contradictions only by adjusting spring stiffness and preload. In addition, improving the stroke frequency is beneficial to ensure large flow rate and high efficiency (Aleksandar *et al.,* 2016). Simultaneously, the requirements for flow rate, pressure and efficiency of reciprocating pump is increasing in some fields. But, the problems, such as fatigue and erosion failure of the valve and spring, become more and more serious with those improvement. And, the greater the stroke frequency, the greater the impact velocity of the valve disc (Pei *et al.,* 2015).

Therefore, considering the striking problems in application, three new structures of the valve are designed in this paper. Based on CFD method, a dynamic simulation model of the valve in suction

stroke is established. Compared with the conventional structure of the valve, the dynamic characteristics, suction performance and internal flow field distribution in the new structures are respectively analyzed.

## 2. NEW PUMP VALVE STRUCTURE

The schematic diagram of hydraulic end of the reciprocating pump is shown in Fig. 1. During the working process of the reciprocating pump, the plunger movement causes the pressure change in the pump chamber, which leads to the suction valve and discharge valve to open and close alternately. Therefore, the performance of the reciprocating pump is obviously affected by the motion characteristics and service life of the valve. Currently, the conventional reciprocating pump generally adopt the structure (valve 1) shown in Fig. 2. The common cylindrical helical spring is used in this structure, and the spring force is approximately linear with the deformation during the valve disc movement. With the increasing requirements for high pressure, large flow rate and high efficiency of reciprocating pumps in some fields, the fatigue failure of the valve disc and spring is becoming more and more prominent.
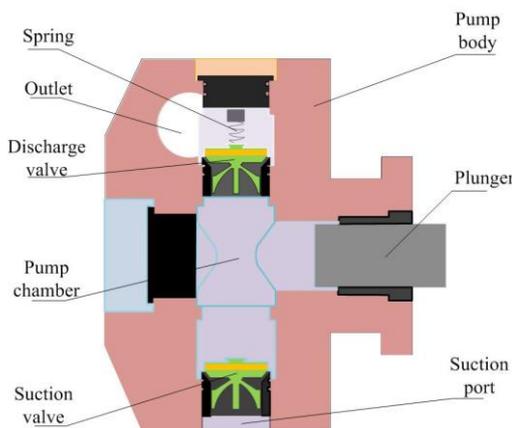


**Fig. 1. Structure diagram of hydraulic end of reciprocating pump.**

In order to solve the above problems, considering the advantages of variable stiffness spring and actual working conditions of the reciprocating pump, three new structures of the valve with variable stiffness are presented as follows:

This valve (valve 2) shown in Fig. 3 is composed of magnetic spring and common cylindrical helical spring. The magnetic poles have the characteristics of mutual exclusion between the same magnetic poles and mutual attraction between the opposite magnetic poles. It can replace common spring to provide restoring force under certain circumstances. Therefore, It is also called magnetic spring. However, the interaction between magnetic poles is only evident at a limited distance. To solve this problem, a combined structure of magnetic spring and common cylindrical helical spring is designed. As shown in Fig. 3, the A and C are the same

magnetic pole, and the corresponding B is the opposite magnetic pole. When the lift is greater than $h_1$, the restoring force of common cylindrical helical springs can be partially offset by the attraction between the magnetic poles. With the further reduction of the distance between the magnetic poles, the effect of magnetic force will be enhanced. The relationship between spring force and deformation can be be expressed as the curve shown in Fig. 3. (The corresponding relationship between them is also called the characteristic line of spring) As shown in Fig. 4, this valve (valve 3) adopts combined spring structure. In this structure, multi-stage springs are connected in parallel. With the change of the lift, the number of working springs can be adjusted to realize the variable stiffness of the valve. This paper only focuses on the three-stage springs, whose characteristic line is shown on the right side of Fig. 4. When the lift is less than $h_1$, only spring provides spring force. When the lift is greater than $h_1$ and less than $h_2$, the two-stage spring provides spring force at the same time, and the spring stiffness increases. When the lift is greater than $h_2$, all springs provide spring force, and the spring stiffness increases further. This structure can achieve variable stiffness, which is beneficial to avoid resonance, and it also has large bearing capacity. In addition, when a spring fails at work, it can still be replaced by other springs. this valve has higher reliability and it can avoid frequent replacement due to spring failure.

The conical spring is used in the valve (valve 4) shown in Fig. 5. Its spring characteristic line is shown on the right side of the Fig. 5. The conical spring is a variable diameter structure. The spring force and deformation of it approximately satisfy the linear relationship before the coil is merged. After the overlay, the spring stiffness increases because the number of effective working coils of the spring decreases (Wu and Hsu, 1998). In other words, with the increase of the number of overlay coils, the spring force caused by unit deformation becomes larger and larger. The variable stiffness characteristic in the deformation process is beneficial to avoid resonance. And it also has large load-carrying capacity and good lateral stability.

## 3. MATHEMATICAL MODEL

### 3.1 Mathematical Model of Plunger Motion

During the working process of reciprocating pump, the rotary motion of crank is transformed into the linear motion of plunger through connecting rod and crosshead, which will cause the change of liquid pressure in the pump chamber. The displacement $x_p$ and velocity $v_p$ of plunger can be expressed as follows:

$$x_p = R(1 - \cos\theta + \frac{1}{2}\lambda\sin^2\theta) \tag{1}$$

$$v_p = R\omega(\sin\theta + \frac{1}{2}\lambda\sin 2\theta) \tag{2}$$

a) Valve structural schematic diagram

b) Spring load and deformation curve
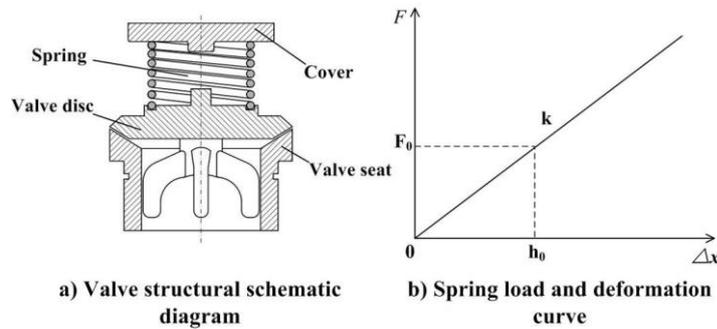
**Fig. 2. Conventional structure (valve 1) and its spring characteristic line.**



a) Valve structural schematic diagram

b) Spring load and deformation curve
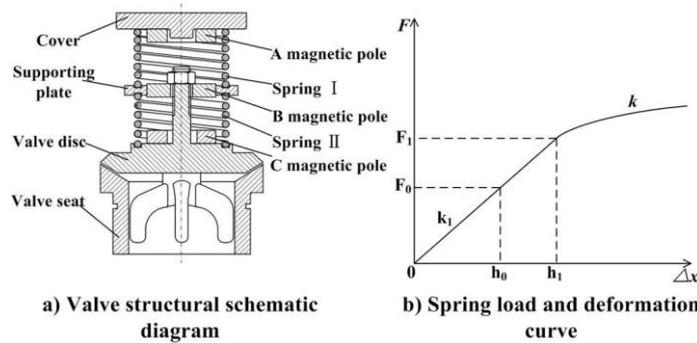
**Fig. 3. New type structure (valve 2) and its characteristic line.**



a) Valve structural schematic diagram

b) Spring load and deformation curve
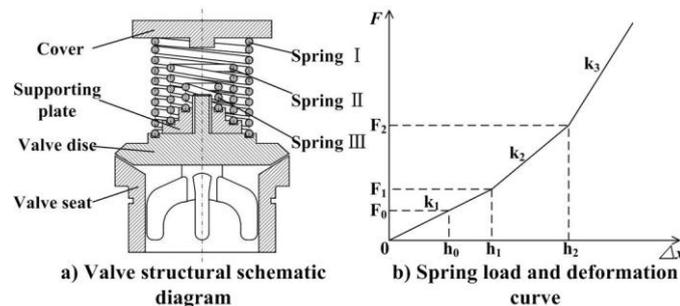
**Fig. 4. New type structure (valve 3) and its characteristic line.**



a) Valve structural schematic diagram

b) Spring load and deformation curve
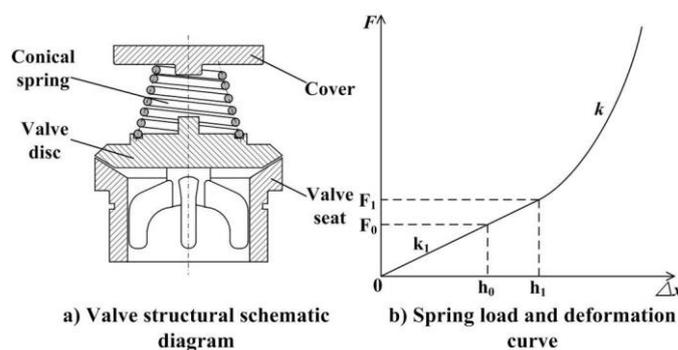
**Fig. 5. New type structure (valve 4) and its characteristic line.**

Where $\lambda$ is the link ratio, $\lambda=R/l$; $l$ is the length of the connecting rod, m;

## 3.2 Mathematical Model of the Valve Disc Motion

In suction stroke, the volume of pump chamber increases due to plunger motion, and the pressure begins to decrease. When the pressure difference is enough to overcome the spring preload and gravity of the valve disc, the suction valve opens. In this process, the valve disc is subjected to the following forces: fluid force produced by the pressure difference acting on its surface, gravity, fluid resistance (This force was eventually omitted), spring force (Qian *et al.,* 2014; Beune *et al.,* 2012;

390

Song *et al.,* 2010). The differential equation of motion of valve disc is as follows:

$$m_s \frac{d^2 h}{dt^2} = F_p - F_s - m_s g \qquad (3)$$

## 3.3 Mathematical Model of Spring Force for Different Valve Structures

Valve 1 shown in Fig. 2 adopts the common cylindrical helical spring. Ignoring the secondary factors of stiffness nonlinearity caused by material and other factors, the relationship between spring force and deformation is generally simplified to a linear relationship, and the spring force satisfies:

$$F_s = k(h + h_0) \qquad (4)$$

Where $k$ is spring stiffness, N/m; $h$ is lift, m; $h_0$ is deformation corresponding to spring preload, m.

Valve 2 is composed of magnetic spring and common cylindrical helical spring shown in Fig. 3. When lift is small, the interaction between magnetic poles is negligible. Only the cylindrical helical spring provides restoring force. The spring force and the deformation are approximately linear. When a certain amount of deformation($h_1$) is reached, the interaction between magnetic poles strengthens and begins to counteract the restoring force of cylindrical helical springs. With the increase of the lift, the counteracting effect is further enhanced. The stiffness decreases with the increase of lift. Similarly, the calculation of spring force during the whole deformation process needs to be considered in segments:

$$F_s = \begin{cases} k_1(h + h_0) & h + h_0 \le h_1 \\ F_1(h + h_0) & h + h_0 > h_1 \end{cases} \qquad (5)$$

Where $k_1$ is the spring stiffness, N/m; $h$ is the lift, m; $h_0$ is the initial deformation of spring; $h_1$ is critical deformation which needs to consider the interaction between magnetic poles, m; $F_1$ is the corresponding function relationship between the spring force and deformation.

Valve 3 adopts combined spring structure shown in Fig. 4. When lift is less than $h_1$, only the spring I provides spring force. When the lift is greater than $h_1$ and less than $h_2$, the two-stage spring provides spring force at the same time. When the lift is greater than $h_2$, all springs provide spring force, so The relationship between spring force and deformation is as follows:

$$F_s = \begin{cases} k_1(h + h_0) & h_0 + h \le h_1 \\ k_1 h_1 + (k_1 + k_2)(h + h_0 - h_1) & h_1 < h_0 + h < h_2 \\ k_1 h_1 + (k_1 + k_2)(h_2 - h_1) + \\ (k_1 + k_2 + k_3)(h + h_0 - h_2) & h_0 + h \ge h_2 \end{cases} \qquad (6)$$

Where $k_1$ is the stiffness of spring I, N/m; $k_2$ is the stiffness of spring II, N/m; $k_3$ is the stiffness of spring III, N/m; $h$ is the lift, m; $h_0$ is the initial deformation of spring, m; $h_1$ is the critical deformation when the intermediate spring II starts to work, m; $h_2$ is the critical deformation when the inner spring III starts to work, m.

The conical spring is used in the valve 4. And its stiffness is approximately constant before the coil overlap. When a certain amount of deformation ($h_1$) is reached, the spring is tightened in turn from the big coil to the small coil. The spring stiffness increases after the coil contacts. And, the spring force and the deformation satisfy a specific functional relationship. Therefore, the calculation of the spring force during the whole deformation process also needs to be considered in segments:

$$F_s = \begin{cases} k_1(h + h_0) & h + h_0 \le h_1 \\ F_2(h + h_0) & h + h_0 > h_1 \end{cases} \qquad (7)$$

Where $k_1$ is the spring stiffness, N/m; $h$ is the lift, m; $h_0$ is the initial deformation of spring, m; $h_1$ is the critical deformation when its coil contacts, m; $F_2$ is the corresponding function relationship between spring force and deformation.

## 3.4 Fluid Governing Equation

The continuity and momentum equations are presented as (Liang *et al.,* 2016):

$$\frac{\partial \rho}{\partial t} + \frac{\partial \rho u_j}{\partial x_j} = 0 \qquad (8)$$

$$\frac{\partial \rho u_i}{\partial t} + \frac{\partial \rho u_i u_j}{\partial x_j} = -\frac{\partial \rho}{\partial x_i} + [(\mu + \mu_t)(\frac{\partial u_i}{\partial x_j} + \frac{\partial u_j}{\partial x_i} - \frac{2}{3}\delta_{ij}\frac{\partial u_k}{\partial x_k})] \qquad (9)$$

Where $\delta_{ij}$ is the Kronecker symbol $\delta_{ij} = 1$ for i = j.

In cavitation, the liquid-vapor mass transfer (evaportation and condensation) is governed by the vapor transport equation:

$$\frac{\partial(\alpha_v \rho_v)}{\partial t} + \nabla \cdot (\alpha_v \rho_v V_v) = S_e - S_c \qquad (10)$$

After cavitation, vapor exists in liquid in the form of bubbles. There is interaction between different phases. To describe the formation, development and rupture of bubbles, it is necessary to study the dynamic characteristics of bubbles. Based on Rayleigh-Plesset equation and considering certain assumptions, the following simplified bubbles dynamic equations can be obtained:

$$\frac{p_v - p}{\rho_1} = R_B \frac{d^2 R_B}{dt^2} + \frac{3}{2}(\frac{d^2 R_B}{dt^2})^2 + \frac{4\mu}{3}\frac{dR_B}{dt} + \frac{2\sigma}{\rho_1 R_B} \qquad (11)$$

Neglecting the secon-order terms, the surface tension term and the viscous term, simplified bubble dynamics Equation can be obtained:

$$\frac{dR_B}{dt} = \sqrt{\frac{2}{3}\frac{|p_v - p|}{\rho_1}} \qquad (12)$$

Considering the mutual transformation between gas phase and liquid phase, the evaporation and condensation terms in Schnerr-Sauer cavitation model are respectively

$$S_e = \frac{\rho_1 \rho_v}{\rho}\frac{3\alpha_v(1 - \alpha_v)}{R_B}\sqrt{\frac{2}{3}\frac{p_v - p}{\rho_1}} \qquad (13)$$

$$S_c = -\frac{\rho_1 \rho_v}{\rho} \frac{3\alpha_v (1-\alpha_v)}{R_B} \sqrt{\frac{2}{3} \frac{p - p_v}{\rho_1}}$$ (14)

The relationship between the volume fraction of gaseous term and the number of voids per unit fluid volume in the model is as follows:

$$\alpha_v = \frac{n_b \frac{4}{3} \pi R_B^{\,3}}{1 + n_b \frac{4}{3} \pi R_B^{\,3}}$$ (15)

## 4. ESTABLISHMENT OF SIMULATION MODEL

### 4.1 Geometric Model

Based on CFD method, this paper mainly studies the movement characteristics of the suction valve and the distribution of the internal flow field during suction stroke. Due to the discharge valve is closed during this process, only the fluid in suction chamber, valve clearance and pump chamber needs to be considered and analyzed (Iannetti *et al.,* 2016). Therefore, the geometric model established of fluid domain is shown in Fig. 6. And, the structural parameters in the modeling process are the same as those of BW-250 horizontal triplex single-acting reciprocating pump (Pei *et al.,* 2016). Its main parameters are as follows: The diameter of plunger is 80 mm, the diameter of suction chamber is 58 mm, the upper surface diameter of the valve disc is 62 mm, and the total volume of pump chamber is $8.9823 \times 10^{-4}$ m³. During the simulation, the discharge pressure is 1 Mpa, and the suction pressure is atmospheric pressure 101325 Pa. In order to compare the performance of new and conventional valves after the stroke frequency is improved, stroke frequency is 300 times/min.
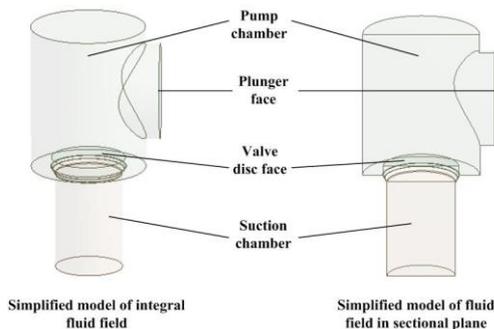


**Fig. 6. Geometric model of fluid domain at the beginning of suction stroke.**

### 4.2 Mesh Generation

Structural mesh have better simulation accuracy, while non-structured mesh have better adaptability. Considering the advantages of both, hybrid mesh is chosen in this paper. The fluid field is divided into three parts. Tetrahedrons mesh is chosen in fluid field I and field III. On the contrary, hexahedral mesh is chosen in fluid field II. Due to requirement that Fluent software must calculate in continuous

flow field, gap between valve disc and valve seat needs to be reserved before at initial time. However, there is no clearance before opening in the real situation. It will affect the pressure drop process in the pump chamber and the motion characteristics of the valve disc in the initial stage. Therefore, a cut-off surface is created shown in Fig. 7. The cut-off surface is wall type before opening and translate into interior type after opening. It can ensure no flow across valve when the valve is closed. In this simulation process, the reserved clearance is 0.5mm. And the mesh at the valve clearance is refined.
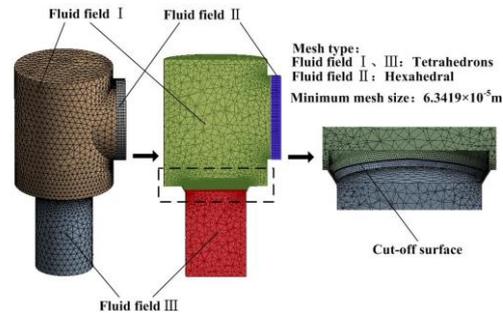


**Fig. 7. Mesh generation in fluid field.**

### 4.3 Dynamic Grid Technology

Because the movement of plunger and valve disc will affect the fluid field during the suction stroke, the mesh of fluid field needs to be updated dynamically according to the position of plunger and valve disc. At the same time, the pressure distribution in the flow field will further affect the motion state of valve disc. Therefore, this paper uses dynamic grid technique and UDF user-defined program to update grid and calculate the motion of valve disc for the purpose of fluid-structure interaction.

The motion of the plunger is mainly determined by the structure parameters and working conditions of the reciprocating pump, so the velocity of the plunger can be determined before the simulation calculation by Eq. (2). The motion of valve disc and its position in the flow field can not be determined in advance, so the motion of the valve disc needs to be calculated according to the flow field distribution near the valve disc in each time step. According to Eq. (3), the acceleration of disc motion at the current time step is as follows:

$$a_t = \frac{F_p - F_s - m_s g}{m_s}$$ (16)

The velocity of valve disc can be expressed as:

$$v_{t+1} = \begin{cases} a_t \Delta t & a_t > 0, z_t = 0 \\ 0 & a_t < 0, z_t = 0 \\ v_t + a_t \Delta t & 0 < z_t < z_{max} \\ 0 & a_t > 0, z_t = z_{max} \\ a_t \Delta t & a_t < 0, z_t = z_{max} \end{cases}$$ (17)

Where $v_{t+1}$ is the valve disc velocity at $t+1$ time

step, m/s; $\Delta t$ is the time step; $z_t$ is the $z$ direction displacement of the valve disc at t time step, m; $z_{max}$ is the maximum displacement in $z$ direction of the valve disc, m.

Similarly, its displacement can be expressed as:

$$z_{t+1} = \begin{cases} 0 & z_{dis} \leq 0 \\ z_{dis} & 0 < z_{dis} < z_{max} \\ z_{max} & z_{dis} \geq z_{max} \end{cases} \quad (18)$$

Where $z_{dis} = z_t + v_{t+1}\Delta t$.

According to Eq. (2), Eq. (14) and Eq. (15), the motion of plunger and valve disc are compiled by UDF. In the simulation process, the dynamic grid is set up by smoothing, layering and remeshing. The Fluid field Ⅰ and Ⅲ in Fig. 7 use remeshing and smoothing to dynamically update the grid deformation caused by the valve disc movement. And fluid field Ⅱ adopts layering method to update the grid deformation caused by plunger movement dynamically. The UDF scheme operations is shown in Fig. 8.
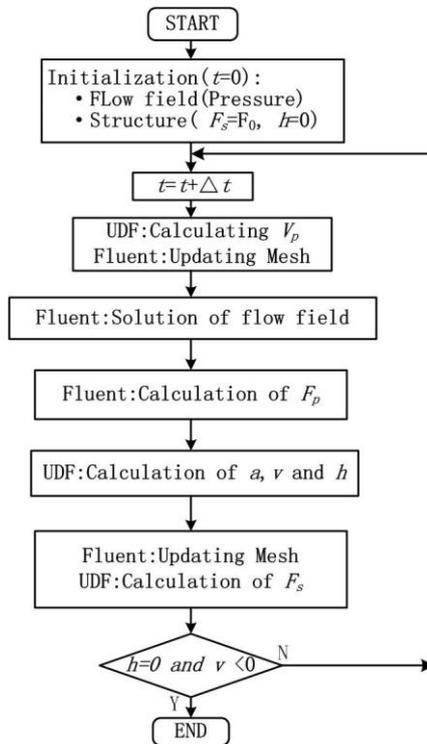


**Fig. 8. Flow chart of UDF scheme operations.**

## 4.4 Computational Details

Considering the actual working conditions, water is selected as working medium. And it is set as compressible fluid. Mixture model is used to set water as the primary phase and water vapor as the secondary phase. Schnerr-Sauer cavitation model is used for the mutual transformation between different phase. Turbulence model plays an important role in CFD simulation process. The selection of it needs to consider flow state, boundary conditions, calculation accuracy, calculation time and other factors. In this paper, the

turbulent flow is complex and diversified in the pump chamber and narrow valve clearance, and changes with time in the working process. Therefore, the Standard k-ε two-equation viscous model with the advantages of most extensive application and reasonable accuracy is adopted in this simulation. Pressure boundary condition is 101325Pa at the inlet of the suction port and the plunger is a moving wall. The velocity of the plunger is determined by Eq. (1). In Fluent, both the segregated (SIMPLE, SIMPLEC, and PISO) and coupled pressure-based solvers can be used in cavitation. As usual, the coupled solver is generally more robust and converges faster (ANSYS Inc., 2016). Therefore, this paper chooses the coupled solver. The initial condition set in this paper is assuming that the discharge stroke has just ended and the discharge valve has been closed. In order to reflect the real opening characteristics of the valve, the fluid domain is initialized under different pressures in different regions. Initial pressure in fluid field Ⅰ and Ⅱ is discharge pressure 1 MPa, and the pressure in fluid field Ⅲ is 101325Pa. The time step needs to be preliminary selected according to the minimum mesh size and the velocity of moving boundary. Then it can be adjusted according to the mesh quality and convergence. The time step in this simulations has been optimized in order to have a good balance between calculation time and accuracy. The final time step is determined to be 0.00001s .

The sensitivity analysis on the grid has performed to determine the optimal scheme which has a good balance between good calculation accuracy and short calculation time. There are several kinds of scheme whose grid numbers are increased gradually from coarse to fine. Figure 9 shows the fluid force acting on the valve disc varies with the number of grid. When the number of grid reaches $13 \times 10^4$, the force has not changed much, which indicates that this grid scheme can meet the calculation requirements while taking less computation time.
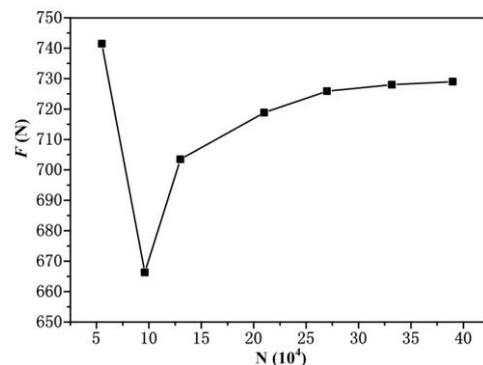


**Fig. 9. Comparisons of force on the valve disc under different grid numbers.**

## 5. RESULTS AND DISCUSSION

Considering the problems mentioned above of valve in practical application, three new structures of the

**Table 1 Spring parameters in different valve structures**

| Type | Spring parameters | | | | |
|---|---|---|---|---|---|
| valve1 | k (N/m) | | | $h_0$ (m) | |
| | 10000 | | | 0.01 | |
| valve2 | $k_1$ (N/m) | F (N) | | $h_0$ (m) | $h_1$ (m) |
| | 10000 | $F_1$ | | 0.01 | 0.01 |
| valve3 | $k_1$ (N/m) | $k_2$ (N/m) | $k_3$ (N/m) | $h_0$ (m) | $h_1$ (m) | $h_2$ (m) |
| | 10000 | 5000 | 5000 | 0.01 | 0.002 | 0.003 |
| valve4 | $k_1$ (N/m) | F (N) | | $h_0$ (m) | $h_1$ (m) |
| | 10000 | $F_2$ | | 0.01 | 0.01 |

Note: The spring force $F_1$ and $F_2$ in the Table 1 are as follows, where x is the sum of the h and $h_0$.

$$F_1 = -6.51 \times 10^9 x^4 + 4.543 \times 10^8 x^3 - 1.034 \times 10^7 x^2 + 1.098 \times 10^5 x - 352.8 \quad F_2 = 0.00327 x^4 + 2.315 \times 10^7 x^3 - 1.354 \times 10^6 x^2 + 2.946 \times 10^4 x - 82.54$$

valve are proposed in this paper. The relationship between spring force and deformation in each valve structure has been established. To compare the performance of different valve structures, four simulation examples are preliminary selected for analysis in this section. The spring parameters selected in the comparison process are shown in Table 1.

## 5.1 Motion Characteristics of the Valve Disc

In the working process of reciprocating pump, fluid flows into or out of the pump chamber through the valve clearance. The flow area of valve clearance will affect the energy loss of fluid passing through the valve. Meanwhile, the lift is an important indicator reflecting the flow area. Besides, when the valve closes, the greater the impact velocity of the disc on the seat, the more serious the fatigue failure of the valve. Therefore, lift and impact velocity can be used as important indicators to reflect the performance of pump valves. Under the same preload condition, Fig. 10 and Fig. 11 are respectively the compare diagrams of lift and velocity of three new valves with conventional ones.
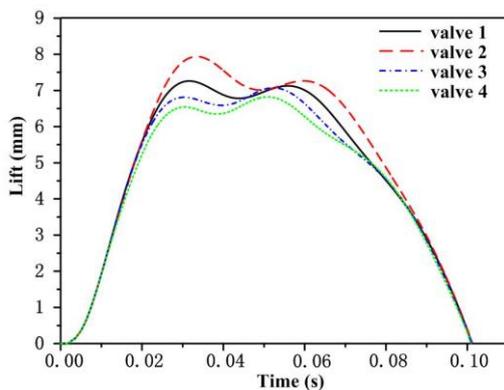


**Fig. 10. Comparison of lift of different valve structures.**

As shown in Fig. 10, there is obvious lag in opening and closing process. This simulation results validate the conclusion of Ma *et al.* (2018). But under the same preload condition, the differences between the four valve structures are not great. The main reason

of opening lag is the compressibility and cavitation of fluid; By comparing the maximum lift, it can be found that valve 2 has the largest one. In other words, it has the largest flow area of valve clearance. Contrasted with conventional valve 1, valve 3 and valve 4 can significantly reduce the maximum lift. The results above show that valve 2 has some advantages in increasing the flow area and reducing the energy loss of fluid passing through it.

During the opening process, the velocity of valve disc quickly reaches its maximum value and then gradually decreases, as shown in Fig. 11. And there is obvious jumping characteristic. When the valve disc descends, there is an acceleration process. In other words, the valve disc will impact the valve seat at a certain velocity. Compared with the velocity curve of conventional valve 1, the impact velocity of valve 3 and valve 4 decreases obviously. But the impact velocity of valve 2 increases slightly. In addition, the velocity fluctuation of valve 2 is the greatest during the whole process. Valve 3 and valve 4 are relatively stable. It can be concluded that valve 3 and valve 4 have a well effect on stabilizing velocity fluctuation.
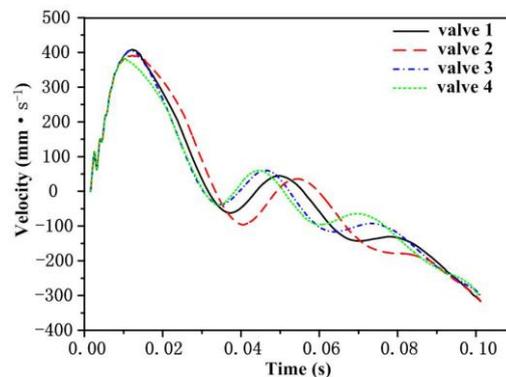


**Fig. 11. Comparison of velocity among different valve structures.**

## 5.2 Flow Field Distribution

During the suction stroke, plunger motion causes pressure drop in pump chamber. And, the fluid will enter the pump chamber through the valve clearance.

Once local pressure in the flow field is less than the
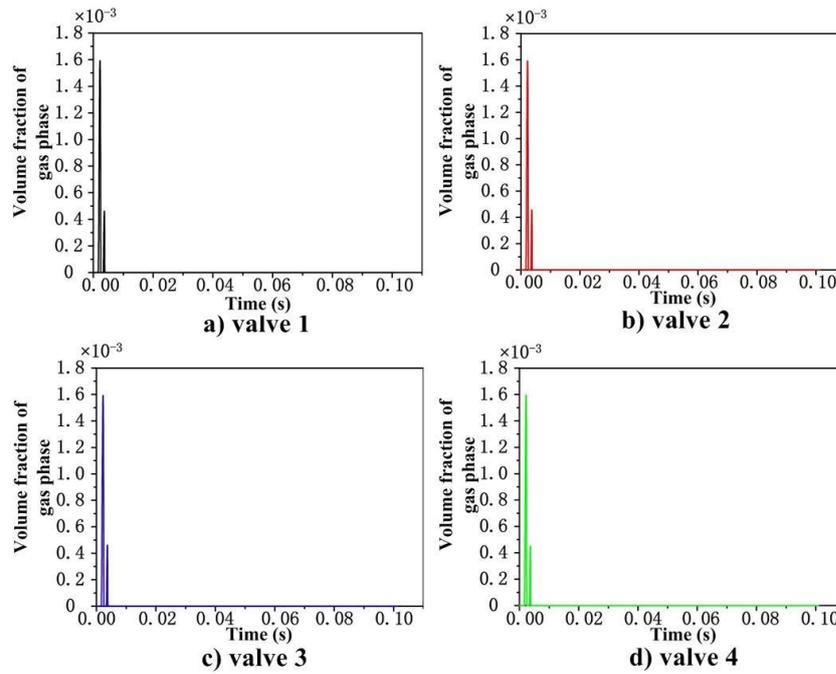
**Fig. 12. Comparison of gas phase volume fraction on plunger surface of different valve structures.**
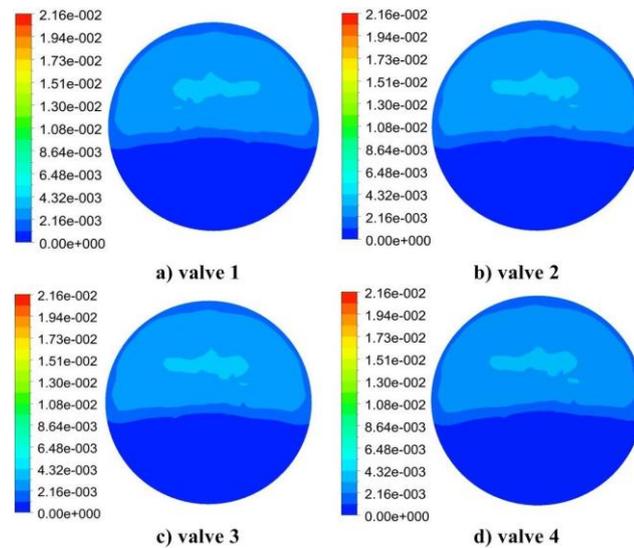


**Fig. 13. Comparison of gas phase distribution contours on plunger surface of different valve structures.**

saturated vapor pressure of this fluid, cavitation will occur. It can reduce the working efficiency of reciprocating pumps, cause erosion damage, and lead to vibration and noise. Besides, the main failure types of the valve in field application are impact fatigue failure and serious erosion failure of the fluid. Therefore, cavitation and flow field distribution will be emphatically analyzed.

### 5.2.1 Comparison of Cavitation Phenomena

After cavitation occurs, the vapor will exist in the form of bubbles. The fluid presents a gas-liquid two phase state. When bubbles reach the high pressure zone, they will burst instantaneously. If the bubble burst near the wall, it will have a significant erosion

effect on it. Considering the failure types of the vulnerable parts in field application, in this simulation process, the cavitation of plunger surface and valve disc surface was monitored. And area-weight average of gas phase volume fraction is recorded. Figure 12 is the comparison diagram of gas phase volume fraction of plunger surface in the different structures of the valve. Figure 13 shows the gas phase contours of the plunger surface at the maximum volume fraction during the suction stroke among different structures of the valve.

It can be seen from Fig. 12 that the maximum volume fraction of the gas phase on the plunger surface occurs at the initial stage of the suction stroke. At this time, the plunger starts to move from
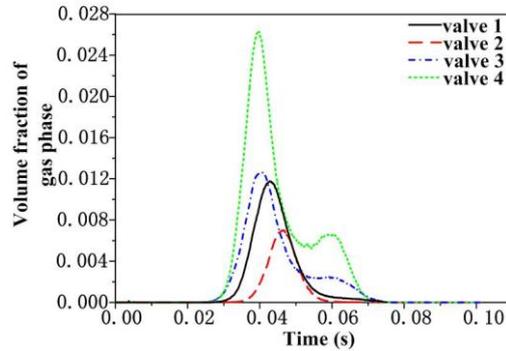
**Fig. 14. Comparison of gas phase volume fraction on valve disc surface of different valve structures.**



a) valve 1

b) valve 2

c) valve 3

d) valve 4
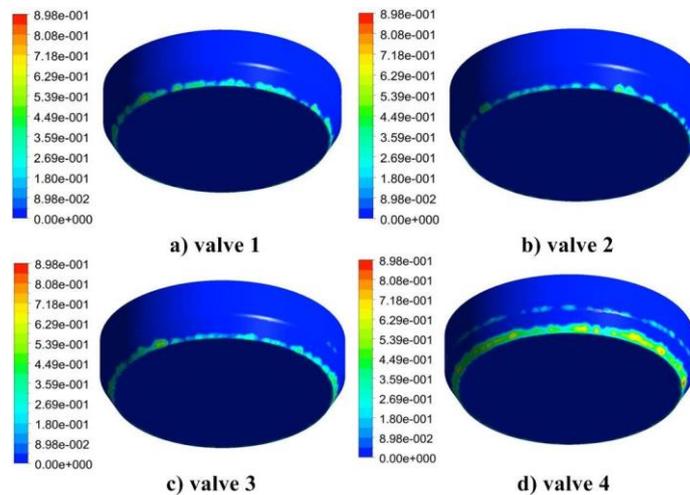
**Fig. 15. Comparison of gas phase distribution contours on valve disc surface of different valve structures.**

the static state. Because of the inertia of the liquid, it does not immediately keep up with the velocity of the plunger. The surface pressure of the plunger decreases. And the local pressure will be lower than the saturated vapor pressure of the liquid, which will cause cavitation. Considering the influence of gravity field, it is found that cavitation mainly occurs on the upper surface of plunger shown in Fig. 13. Simultaneously, the duration of cavitation is very short and the value of volume fraction of gas phase is small. Comparing the four structures of the valve, under the same stroke frequency and spring preload, the cavitation of plunger surface has little difference.

Figure 14 shows the variation of gas volume fraction over time on the surface of the valve disc with different structure during the suction stroke. Its value reaches maximum in the middle stage of suction stroke. Certainly, the cavitation is more serious at this time. The gas volume fraction and duration of cavitation in different structures of the pump valve are obviously different. Compared with Conventional valve 1, valve 2 can reduce the duration of cavitation and the value of gas volume fraction. The effect of valve 3 and valve 4 is just the opposite. Among them, valve 4 has the most serious

cavitation in the suction stroke.

Figure 15 and Figure 16 are respectively the gas phase distribution contours and pressure distribution contours when the gas phase volume fraction on the surface of the valve disc is maximum. As can be seen from Fig. 16, there are two distinct annular low pressure regions at the inlet and outlet of the valve clearance. However, the low pressure and cavitation at the inlet are more obvious than those at the outlet. Certainly, cavitation on the surface of the valve disc mainly occurs in these areas. Compared with conventional valve 1, the low pressure and cavitation areas of valves 3 and 4 are more obvious, And the annular cavitation area of valve 4 is larger. From the view of design and optimization of the valve, these areas need to be studied emphatically.

### 5.2.2 Comparison of Fluid Velocity

It is shown in Fig. 17 that the comparison of maximum flow velocitiy in fluid field with different structures of the valve. The flow velocity reaches its maximum in the middle of the suction stroke. Moreover, the maximum velocitiy of valve 2 is generally lower than that of the other three structures. However, the maximum flow velocity of valve 3 and 4 are larger than that of valve 1 as a
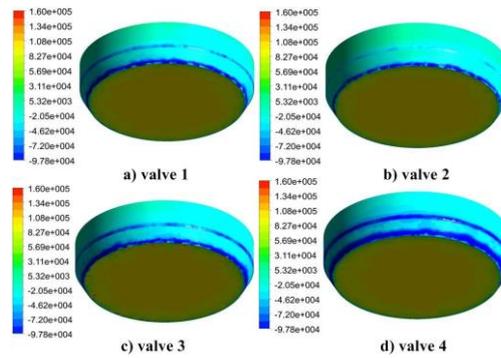
**Fig. 16. Comparison of pressure distribution contours on valve disc surface of different valve structures.**
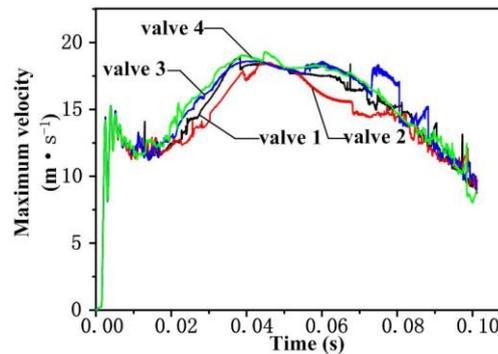


**Fig. 17. Comparison of maximum velocity in valve clearance of different valve structures.**
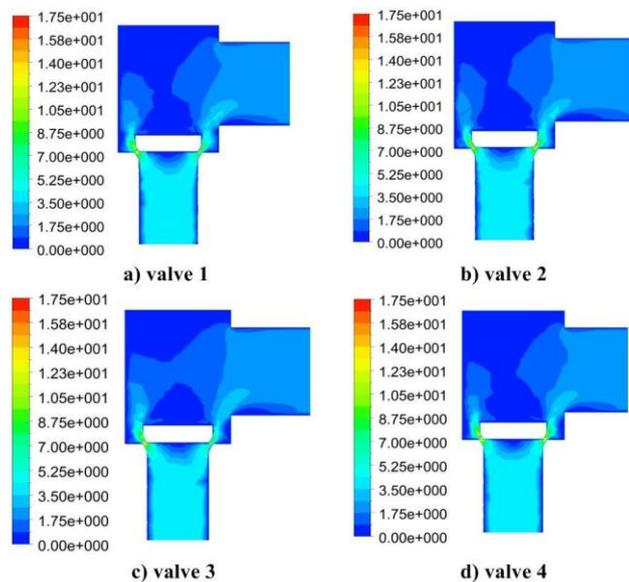


**Fig. 18. Comparison of velocity distribution contours of different valve structures.**

whole. Velocity distribution contours corresponding to maximum velocity is shown in Fig. 18. It shows that the maximum velocitiy in the fluid field occurs in the valve valve clearance. The flow velocity in this area is high. Certainly, the erosion damage to the surface of the valve disc and the valve seat is more serious. Reducing the flow velocity in the valve clearance is conducive to improving the service life of the valve. By comparison, the effect of valve 2 is the most obvious.

### 5.2.3 Comparison of the Pressure in Pump Chamber

During the simulation of different structures of the valve, the pressure change at the same point in the pump chamber was monitored. Their comparison results are shown in Fig. 19. It can be seen that,
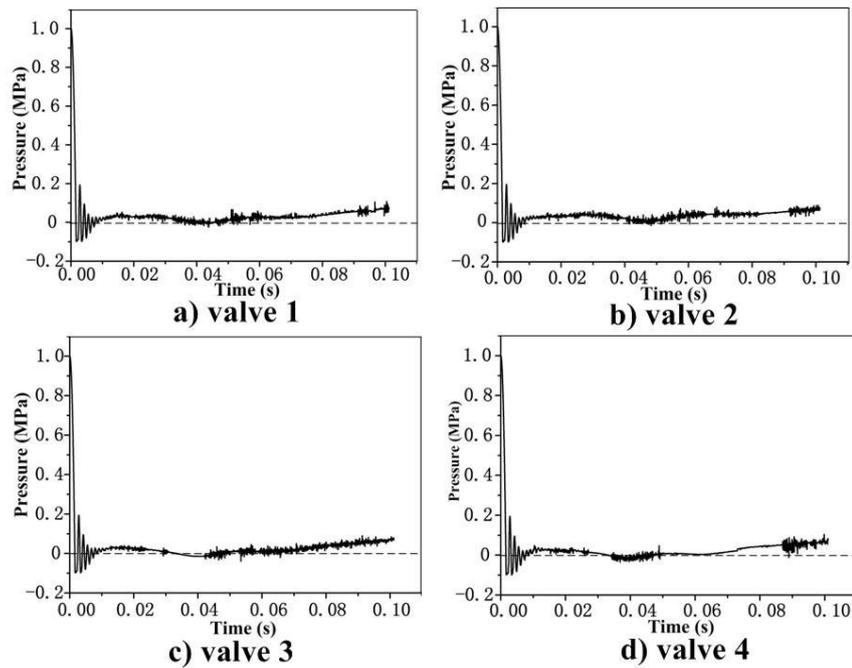
**Fig. 19. Comparison of pressure in pump chamber of different valve structures.**

with the motion of the plunger, the pressure in the pump chamber decreases from the discharge pressure. At the initial stage of the valve opening, the pressure in pump chamber fluctuates to some extent. Subsequently, the fluctuations gradually stabilized. Comparing with the conventional structures, the pressure of valve 3 and valve 4 is lower than that of valve 1 in the middle stage of suction stroke. Valve 2, however, is the opposite. Figure 20 shows the spectrum of the pressure signal in the pump chamber. The fast fourier transform (FFT) of their pressure signals coincides near the pump operating frequency of 5 Hz. Compared with valve 1, the low frequency part of valve 2 has larger amplitude, while the high frequency part of valve 3 and valve 4 has larger amplitude. Low frequency has a greater impact on the stability of the valve. Therefore, the stability of valve 3 and 4 is better.

## 5.4 Verification of Simulation Results

In order to compare the computational accuracy of different simulation methods about the motion of valve, Pei *et al.* (2016) established an experimental system. A BW-250 horizontal triplex reciprocating pump was chose as the testing pump. The inductance frequency-modulation displacement and the piezoelectric accelerometer sensor were installed on the valve disc to directly obtain corresponding motion parameters. In this paper, the same structure parameters were used in the process of establishing simulation model. And the same operation parameters were used in the calculation process as the simulation parameters. The simulation results were compared with the experimental results to verify the simulation accuracy. The maximum lift of the valve disc under different stroke frequency was selected. The comparison results are shown in Table 2. It shows

that the maximum simulation error is less than 8%. The simulation result satisfies the actual accuracy requirement of engineering well.
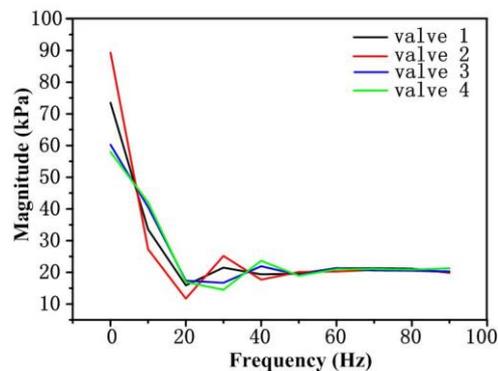


**Fig. 20. FFT of the pressure in pump chamber of different valve structures.**

**Table 2 Simulation and experiment comparison of maximum lift**

| Stroke frequency | 42 | 72 | 116 | 200 |
|---|---|---|---|---|
| Simulation(mm) | 2.377 | 4.181 | 6.223 | 9.907 |
| Experiment(mm) | 2.529 | 4.271 | 6.557 | 10.690 |
| Error | 6.01% | 2.10% | 5.09% | 7.32% |

## 6. CONCLUSION

In this paper, three new structures of the valve are designed and their working principles are briefly

introduced. Furthermore, based on CFD method, a three-dimensional dynamic simulation model considering fluid-structure interaction in suction stroke is established by using dynamic grid technique and UDF. Through this simulation method, the performance of the new valve is compared with that of the conventional valve. Besides, comparing the simulation results and experimental results of the maximum lift of the valve disc, it is found that they are in good agreement. The accuracy of the simulation results is verified. The following conclusions are drawn:

1) The simulation results show that cavitation can be observed on both plunger and valve disc surfaces during the suction stroke. However, the plunger surface cavitation occurs in the initial stage of the suction stroke. It lasts for a short time and concentrates on the upper half of plunger surface; Cavitation on the surface of the valve disc occurs most of the time during the suction stroke, and it is most obvious when the fluid velocity between the valve clearances reaches its maximum. Simultaneously, the cavitation area on its surface is mainly concentrated in the annular area near the inlet and outlet of the valve clearances. Comparatively, it is more serious near the inlet. Therefore, in order to prevent the erosion caused by cavitation, the above areas can be emphatically protected.

2) Compared with conventional valve 1, under the same spring preload, the lift of valve 2 increases significantly and the maximum flow velocity between valve clearance decreases obviously. In addition, the degree of cavitation on the surface of the valve disc is reduced. Therefore, it is beneficial to reduce erosion failure. Although the impact velocity is slightly increased, it has little effect on the service life of the valve when it meets the design requirements. Valve 3 and valve 4 have better stability during the process of movement, and stronger bearing capacity under high pressure conditions. Contrary to the characteristics of valve 2, they can reduce impact velocity but increase the flow velocity of valve clearance and the degree of cavitation.

3) In view of the problems of pump valve in practical application, a new solution with variable spring stiffness is proposed in this paper. The new structures of the valve based on this are also designed. These new structures can provide a new research direction for improving the performance of reciprocating pumps. Simultaneously, the above simulation methods can provide some guidance for design, structural optimization and service life improvement of the valve.

4) In this paper, three new structures of the valve are proposed, and their performance is preliminarily analyzed and compared. According to specific application conditions,

it is necessary to further study the optimal design of type and size.

## REFERENCES

Aleksandar,J., J.J.Roberts,J. Corney, B. Davies and Z. K. Shipton (2016). Reducing the environmental impact of hydraulic fracturing through design optimisation of positive displacement pumps. *Energy* 115, 1216-1233.

ANSYS Inc (2016). Ansys Help 17.0: Fluent theory guide.

Beune, A., J. G. M. Kuerten and M. P. C. van Heumen (2012). CFD analysis with fluid–structure interaction of opening high-pressure safety valves. *Computers & Fluids* 64, 108-116.

Deng,H.,Y. Liu, P. Li and S. Zhang (2018a). Hybrid model for discharge flow rate prediction of reciprocating multiphase pumps. *Advances in Engineering Software* 124, 53-65.

Deng, H.,Y. Liu, P. Li and S. Zhang (2018b). Active learning for modeling and prediction of dynamical fluid processes. *Chemometrics and Intelligent Laboratory Systems* 183, 11-22.

Deng, H.,Y. Liu, P. Li,Y.Ma and S. Zhang (2018c). Integrated probabilistic modeling method for transient opening height prediction of check valves in oil-gas multiphase pumps. *Advances in Engineering Software* 118, 18-26

Deng, H., Y. Zhang, B. Chen,Y.Liu and S. Zhang (2019). Special Probabilistic Prediction Model for Temperature Characteristics of Dynamic Fluid Processes. *IEEE Access* 7, 55064-55072.

Iannetti, A., M. T. Stickland and W. M. Dempster (2016). A CFD and experimental study on cavitation in positive displacement pumps: Benefits and drawbacks of the 'full' cavitation model. *Engineering Applications of Computational Fluid Mechanics* 10(1), 57-71.

Kaya, M. and E. Ayder (2017). Prediction of Cavitation Performance of Radial Flow Pumps. *Journal of Applied Fluid Mechanics* 10(5), 1397-1408.

Lee, J. K., J. K.Jung, J. Chai and J. W. Lee (2015). Mathematical modeling of reciprocating pump. *Journal of Mechanical Science and Technology* 29(8), 3141-3151.

Liang, J., X. Luo, Y. Liu, X. Li and T. Shi (2016). A numerical investigation in effects of inlet pressure fluctuations on the flow and cavitation characteristics inside water hydraulic poppet valves. *International Journal of Heat and Mass Transfer* 103, 684-700.

Luo, X., B. Ji and Y. Tsujimoto (2016). A review of cavitation in hydraulic machinery. *Journal of Hydrodynamics* 28(3), 335-358.

Ma,Y., Y. Ni, H. Zhang, S. Zhou and H. Deng (2018). Influence of valve's lag characteristic on pressure pulsation and performance of reciprocating multiphase pump. *Journal of Petroleum Science and Engineering* 164, 584-594.

Opitz, K. and E. Schlücker (2010). Detection of Cavitation Phenomena in Reciprocating Pumps using a High-Speed Camera. *Chemical Engineering & Technology* 33(10), 1610-1614.

Pei J., H. Chao, L. Miaorong, X. Huang, K. Shen and K. Bi (2016). The valve motion characteristics of a reciprocating pump. *Mechanical Systems and Signal Processing* 66(67), 657-664.

Qian, J., L.Wei, Z. Jin, J. Wang, H. Zhang and A. Lu (2014). CFD analysis on the dynamic flow characteristics of the pilot-control globe valve. *Energy Conversion and Management* 87, 220-226.

Saha, B. K, H. Chattopadhyay, P. B. Mandal and T. Gangopadhyay (2014). Dynamic simulation of a pressure regulating and shut-off valve. *Computers & Fluids* 101, 233-240.

Singh P., J., K. Madavan Nateri (1987). Complete analysis and simulation of reciprocating pumps including system piping. In *Turbomachinery and Pump Symposia*, Texas.

Song, X. G., L. Wang, Park Y. C. (2010). Transient Analysis of a spring-loaded pressure safety valve using computational fluid dynamics (CFD). *Journal of Pressure Vessel Technology-transactions of the Asme* 132(5), 1-5

Wang, G., L. Zhong, X. He, Z. Lei, G. Hu, R. Li and Y. Wang (2015). Dynamic behavior of reciprocating plunger pump discharge valve based on fluid structure interaction and experimental analysis. *Plos One* 10(10), 1-20.

Wu W. H. and Hsu W. Y. (1998). Modelling the static and dynamic behavior of a conical spring by considering the coil close and damping effects. J*ournal of Sound and Vibration* 214(1), 17-28.

Yang, G., Y. Xin, S. Zheng and H. Cong (2010). Particle image velocimetry measurement of the flow field in the play of the drilling pump valve. *Chinese Journal of Mechanical Engineering* 23(1), 27-37.